RSC Advances

PAPER

Cite this: *RSC Adv.*, 2016, **6**, 85202

# A novel graphene oxide coated biochar composite: synthesis, characterization and application for Cr(VI) removal

Mei-rong Shang,[ab] Yun-guo Liu,*[ab] Shao-bo Liu,[c] Guang-ming Zeng,[ab] Xiao-fei Tan,[ab] Lu-hua Jiang,[ab] Xi-xian Huang,[ab] Yang Ding,[ab] Yi-ming Guo[d] and Shu-fan Wang[ab]

In the current work, a graphene oxide coated water hyacinth biochar composite (WHB-GO) was synthesized to remove Cr(VI) from aqueous solution. The biomass feedstock was firstly treated with graphene oxide and then annealed at 300 °C in a quartz tube furnace under $N_2$ atmosphere. After synthesis, full characterization with various techniques (SEM, FT-IR, XPS and BET) were used to analyze the properties of the adsorbent and the sorption mechanisms of Cr(VI). The effects of pH, ionic strength, sorption kinetics, isotherms and thermodynamics, as well as comparison and regeneration experiments were also investigated. The results indicated that the adsorption capacity was significantly influenced by pH and ionic strength. The maximum adsorption capacity (150.02 mg $g^{-1}$) of the WHB-GO was obtained at pH 2.0 and 50 °C. Besides, the sorption data could be fitted well by pseudo-second-order and Freundlich models. The thermodynamic studies indicated that the adsorption reaction was a spontaneous and endothermic process. The enhanced adsorption of Cr(VI) on the WHB-GO was mainly controlled by electrostatic attraction and reduction of Cr(VI) coupled with Cr(III) complexation. The regeneration study revealed that WHB-GO could be reused almost six times without loss of activity in adsorption tests. Overall, WHB-GO can be used as a novel, facile, and low-cost sorbent for the removal of Cr(VI) from aqueous solution.

Received 18th March 2016
Accepted 27th August 2016

DOI: 10.1039/c6ra07151a

www.rsc.org/advances

## 1. Introduction

In recent years, heavy metal ions at high concentrations in water systems have posed a potential threat to human beings and living organisms due to their bioaccumulation and decomposition difficulty in food chains.[1] Chromium is one of the most widespread heavy metals in the environment. As a major pollutant, chromium mainly exists in two stable forms in water: Cr(III) and Cr(VI).[2] However, Cr(VI) is especially poisonous, which was 100 times greater than Cr(III) in toxicity. Thus, hexavalent chromium can cause many serious health problems for human beings (*e.g.*, skin irritations, lung cancer, and viscera damage).[3] So, developing an effective method to remove Cr(VI) from effluent is of great importance to the public health and ecological system. Until now, the methods of removing Cr(VI) are miscellaneous, such as electrocoagulation,[4] reverse osmosis (RO),[5] ion exchange,[6] redox reaction,[7] membrane separation,[8] and adsorption.[9] Among these methods, adsorption is one of the most popular and effective option, due to its cost-effectiveness, simple operation and least waste generation.[10]

Biochar is an easily acquiring adsorbent, which has been increasingly used to eliminate Cr(VI) in recent years. Deveci *et al.*[11] reported that coconut shell-based and coal-based activated carbons were commonly used as adsorbents for Cr(VI) removal. Mohan, Sarswat, Ok *et al.*[12] also illustrated Cr(VI) could be removed from water *via* various adsorbents such as sugar beet tailing biochar, oak wood char and oak bark char. The previous studies have illustrated that water hyacinth is a free floating aquatic and recalcitrant weed which has been spread throughout the world.[13] The uncontrolled growth of water hyacinth has a number of negative impacts, such as interference with fishing generation, obstruction of river courses, reservoirs and water channels and increasing evapo-transpiration.[13] Therefore, the biochar derived from water hyacinth following by application in the treatment of Cr(VI)-contaminated water might represent an attractive pathway for removing Cr(VI) ions from water and improve management of this highly problematic invasive species.[14] However, biochar produced directly from biomass feedstock without any pretreatment has

[a]*College of Environmental Science and Engineering, Hunan University, Changsha 410082, P. R. China. E-mail: liuyunguo824@sina.com; Fax: +86 731 88822829; Tel: +86 731 88649208*

[b]*Key Laboratory of Environmental Biology and Pollution Control (Hunan University), Ministry of Education, Changsha 410082, P. R. China*

[c]*College of Metallurgy and Environmental Research, Central South University, Changsha 410004, P. R. China*

[d]*School of Economics and Management, Shanghai Maritime University, 1550 Haigang Ave, Shanghai 201306, P. R.China*

relatively low adsorption capacity. Thus, various modification/activation methods have been applied to improve the adsorption performance of biochar. Previous studies have been reported that several methods, such as acid and alkali modification, oxidation, and chemical graft, have been used to improve their functional group contents and enhance their adsorption performance.[15,16] However, these previous modified biochar have some disadvantages: such as non-ideal adsorption capacity, occurrence of secondary pollution during production, low reutilization rate and high price.[17] Thus, it is necessary to develop an efficient, environmentally friendly and low-cost adsorbent to remove Cr(VI) from aqueous solution.

Nowadays, graphene oxide (GO) has attracted vast technological and scientific interest due to its specific properties, such as multiple oxygen-containing functional groups (hydroxyl, epoxide, carbonyl and carboxyl groups), large specific surface areas and hydrophilicity.[18,19] At present, researchers have proved that GO could be a promising material to adsorb pollutants from water, such as dyes,[20,21] heavy metals,[22] polycyclic aromatic hydrocarbons (PAHs)[23] and endocrine disruptor chemicals (EDCs). In addition, GO could be easily obtained from many methods[24,25,] which provides a potential, cost-effective and large-scale production. Moreover, GO shows fine biocompatibility.[26] Due to the above-mentioned excellent properties of graphene oxide, it is believed that it could be used as coating material to functionalize various adsorbent. However, GO disperses poorly in water and easily aggregates, causing its surface areas to decrease and limiting its applicability. Therefore, attention has been focused on integrating GO with other materials by fabricating composites to enhance its applicability in the environment.[27] Therefore, in this work, a new composite was synthesized by taking advantage of the recent methods in graphene oxide and biochar technologies.

In this study, a novel functional adsorbent, graphene oxide coated biochar, was prepared by slow pyrolysis in tube furnace at 300 °C. After systematic characterization (SEM, FT-IR, XPS, BET and zeta-potential) of its structural properties, a new-type resultant material was applied for removal of Cr(VI) from solution. Batch experiments were carried out to study the effects of pH, ionic strength and temperature on Cr(VI) adsorption. The kinetics, isotherms and thermodynamics were also utilized to evaluate the adsorption properties for Cr(VI) by graphene oxide coated water hyacinth biochar composite (WHB-GO). Additionally, the desorption experiment and adsorption mechanism were also elucidated.

# 2. Materials and methods

## 2.1 Materials

All chemicals used in this work were of analytical grade, including HCl (hydrochloric acid), NaOH (sodium hydroxide), $H_2SO_4$ (concentrated sulfuric acid), $KMnO_4$ (potassium permanganate), $NaNO_3$ (sodium nitrate), $H_2O_2$ (hydrogen peroxide), $K_2S_2O_8$ (potassium persulfate), $P_2O_5$ (phosphorus pentoxide) and $K_2Cr_2O_7$ (potassium dichromate). Synthetic graphite powder was purchased from Sigma-Aldrich. Water hyacinth was collected from Ocean Lake Wetland Park of Changsha, China. The materials were dried at 105 °C for 12 h and then milled into powders by a high speed rotary machine prior to use.

## 2.2 Preparation of graphene oxide suspension

Stable graphene oxide suspension was prepared from the synthetic graphite powder by using a method similar to modified Hummers method.[28] Briefly, graphite powder (3.0 g) was firstly preoxidized by concentrated $H_2SO_4$ (12 mL) $P_2O_5$ (2.5 g) and $K_2S_2O_8$ (2.5 g) at 80 °C for 4.5 h. Then, the concentrated $H_2SO_4$ (120 mL), $KMnO_4$ (15 g) and $NaNO_3$ (2.5 g) were used to oxidize the preoxidized graphite. After that, 20 mL $H_2O_2$ (30 wt%) solution was added to eliminate the excess $MnO_4^-$, and the products were rinsed repeatedly with HCl (10%) and ultrapure water. The obtained solution was sonicated for 2 h and stored in a refrigerator at 4 °C before use.

## 2.3 Preparation of adsorbent

The graphene oxide suspension was firstly coated on the water hyacinth powders using a dip coating procedure which was similar to the previously reported.[29] Briefly, 10 g water hyacinth biomass was dipped into the graphene oxide suspension (mass ratio = 1 : 0.06 g) and was stirred for 1 h using a magnetic stirrer at 500 rpm. After that, the dip-coated GO raw materials were sonicated for 2 h to promote mix well and then oven dried at 80 °C. Finally, the obtained materials were placed in tubular furnace to produce the graphene oxide-coated biochar through slow pyrolysis in a $N_2$ environment at temperature of 300 °C for 2 h. Untreated water hyacinth powders were also used as feedstock to produce biochar without graphene oxide coating in the furnace with the same pyrolysis conditions. The obtained adsorbent samples were washed with ultrapure water for several times to remove impurities, then vacuum dried and sealed in a desiccator for further experiment tests. The GO coated water hyacinth biochar composite and pristine water hyacinth biochar were labeled as WHB-GO and WHB, respectively.

## 2.4 Materials characterization

The scanning electron microscopy (SEM) (JSM-7001F, Japan) analysis was carried out to determine the surface morphologies and microscopic features of prepared materials. The Fourier transform-infrared technique (FT-IR) (Nicolet 5700 Spectrometer, USA) was used to determine the functional groups on the surface of adsorbents before and after contacting with Cr(VI) ions. The elements of the samples were performed by an ESCALAB 250Xi X-ray Photoelectron Spectrometer (XPS) (Thermo Fisher, USA). The total surface areas and aperture of materials were determined by the method of Brunauer, Emmett, and Teller (BET) (Tri-star 3020, USA). WHB and WHB-GO samples were analyzed by BET using nitrogen as adsorptive gas to characterize the surface area and total pore volume.

## 2.5 Adsorption experiment

A stock solution of Cr(VI) (1000 mg $L^{-1}$) was prepared by dissolving 2.8290 g potassium dichromate ($K_2Cr_2O_7$) into 1000 mL

ultrapure water. In batch experiments, the different Cr(VI) concentrations were obtained by diluting the stock solution. All adsorption experiments were performed in sealed 100 mL glass conical bottles that contained 0.1 g of WHB-GO and 50 mL of a Cr(VI) solution in an appropriate concentration. The bottles were placed in a shaking water bath with a shaking speed of 150 rpm for 24 h. The pH of Cr(VI) solutions was adjusted to obtain the desired values by adding negligible volumes of NaOH and HCl (0.1–0.8 mol $L^{-1}$).

The effect of pH on the adsorption of Cr(VI) was studied with an initial Cr(VI) concentration of 100 mg $L^{-1}$ in a pH range of 2.0 to 9.0 (2.0, 2.5, 3.0, 4.0, 5.0, 6.0, 7.0, 8.0 and 9.0) at 30 °C. The zeta potentials of WHB-GO were measured in aqueous solutions at pH 2.0 to 10.0 by Zetaplus 90 (Brook-haven Instruments, New York, USA). The effect of the ionic strength on the adsorption of Cr(VI) was studied by adding NaCl to 100 mg $L^{-1}$ Cr(VI) solutions with concentrations ranging from 0 to 1 mol $L^{-1}$ (0, 0.001, 0.005, 0.01, 0.005, 0.1, 0.5 and 1 mol $L^{-1}$) at 30 °C and pH 2.0. An adsorption kinetic study was carried out with an initial Cr(VI) concentration of 100 mg $L^{-1}$ at 30 °C and pH 2.0 to determine the minimum time required for equilibrium adsorption. The concentrations of Cr(VI) were measured at different time intervals from 15 to 2880 min (15, 30, 60, 120, 180, 360, 480, 600, 720, 1080, 1440, 2160 and 2880 min). To evaluate the maximum adsorption capacity and thermodynamic properties, adsorption isotherms of Cr(VI) on WHB-GO were obtained at pH 2.0 at 30 °C, 40 °C and 50 °C, respectively. The initial Cr(VI) concentrations ranged from 100 to 800 mg $L^{-1}$ (100, 200, 300, 400, 500, 600, 700 and 800 mg $L^{-1}$). Furthermore, in order to better highlight the superiority of WHB-GO adsorption performance, WHB and water hyacinth biomass as adsorbent were also studied. In particularly, the different concentrations of initial Cr(VI) solution were shaken at pH 2.0 and 30 °C. The remaining concentration of Cr(VI) was determined by using a UV spectrophotometer (Pgeneral T6, China) at a wavelength of 540 nm. The adsorption capacity ($q_e$ (mg $g^{-1}$)) and removal efficiency ($E_R$) of tested adsorbents at the equilibrium state was calculated by the following equations:

$$q_e = \frac{(C_0 - C_e)v}{w} \quad (1)$$

$$E_R = \frac{C_0 - C_e}{C_0} \times 100\% \quad (2)$$

where $v$ (L) is the volume of solution, $w$ (g) is the amount of adsorbent, $C_0$ and $C_e$ (mg $L^{-1}$) are the initial and equilibrium concentrations of Cr(VI), respectively.

# 3. Result and discussion

## 3.1 Characterization of adsorbents

**3.1.1 SEM.** The surface morphologies of WHB, WHB-GO before and after adsorption of Cr(VI) were displayed in the SEM images. As seen from Fig. 1(a), WHB showed uneven and irregular surface, meanwhile a lot of carbon particles were also observed from the surface of the pristine biochar, which indicated that the water hyacinth were pyrolyzed and carbonized.

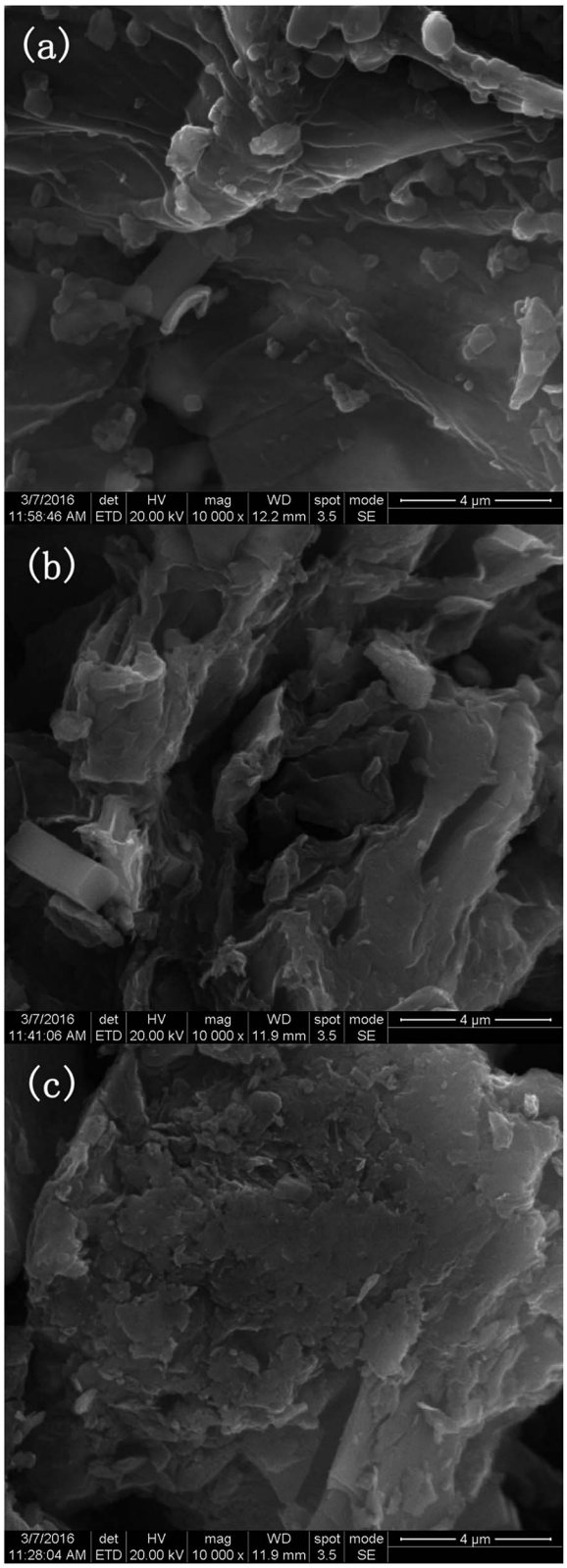


Fig. 1 SEM images of WHB (a), WHB-GO (b), and after adsorption of Cr(VI) on WHB-GO (c) (WHB-GO + Cr).

However, after coating with GO, there was a visible change, the WHB-GO (Fig. 1(b)) showed sheet-like structure with thick sheets and wrinkled edges, which could present a higher

 

surface area and provide effective adsorption sites. After reaction with Cr(VI), the composite became much more smooth and well-knit (Fig. 1(c)). This phenomenon was possibly due to the adsorption of Cr(VI) onto the surface of adsorbent that blocked the pore channel.

**3.1.2 FT-IR.** The FT-IR technique was used to determine the functional groups on the surface of WHB and WHB-GO (before and after adsorption) and the results were presented in Fig. 2. The spectra of both WHB and WHB-GO emerged a number of adsorption peaks indicating the relative complex of the materials. For the two carbon materials, the characteristic peak at 3423.0 $cm^{-1}$ was attributed to the C=O in the hydroxyl groups. The bands at around 1610.3 $cm^{-1}$ and 1319.0 $cm^{-1}$ were assigned to C–C and C–OH stretching vibration.[20] No obvious peak between 1200 $cm^{-1}$ and 450 $cm^{-1}$ could be found in the spectrum of WHB. Compared with the spectrum of WHB, more peaks occurred in the spectra of WHB-GO. The appearance of new peaks at 520.7 and 470.5 $cm^{-1}$ in the spectrum were attributed to C–H and C–O stretching vibration. The new strong peaks at 1033.7 and 781.0 $cm^{-1}$ in the spectrum of WHB-GO were attributed to the stretching of C–O–C and aromatic compounds, respectively.[30] In short, the adsorption peak of C–H, C–O, C–O–C and aromatic compounds groups changed after modification, which confirmed that the surface carbon functional groups of the GO were successfully introduced into the composites during the pyrolysis process in the tube furnace. Therefore, the information given by the FTIR spectra proves that WHB-GO was prepared successfully. Additionally, the detailed description of WHB-GO loaded with Cr (WHB-GO + Cr) will be discussed in the following section concerning the adsorption mechanism.

**3.1.3 XPS.** In order to gain further information on its chemical composition, XPS (X-ray photoelectron spectroscopy) analysis was performed on WHB-GO before and after its reaction with Cr(VI) and the results were exhibited in Fig. 3. In the XPS survey, the principal elements at WHB surface were carbon (69.91%), oxygen (23.86%), nitrogen (4.56%) and phosphorus (1.67%) and at WHB-GO surface were carbon (66.79%), oxygen (29.55%), nitrogen (3.18%) and phosphorus (0.48%). It demonstrated that the existence of carbon and oxygen composed the main body of the two materials. Obviously, the ratio of carbon content to oxygen content (C/O) for WHB and WHB-GO were 2.93 and 2.26, respectively, which implied that more oxygen-containing functional groups, such as C=O, C–O are introduced.

Detailed XPS surveys of the regions for $Cr_{2p}$ were shown in Fig. 4. The high-resolution spectra of Cr-laden biomaterials indicated that there were significant contributions of the Cr bound on their surfaces. The $Cr_{2p}$ XPS spectrum of WHB-GO, significant peaks centered at 575–577 and 585–588 eV were observed, which corresponded to Cr $2p_{3/2}$ orbitals and Cr $2p_{1/2}$ orbitals, respectively. The Cr $2p_{3/2}$ orbitals were assigned at 577.2 eV ($CrCl_3$) and 575.2–576.5 eV ($Cr_2O_3$) for Cr(III) compounds, while Cr(VI) forms were characterized by higher binding energies such as 578.1 eV ($CrO_3$) or 579.2 eV

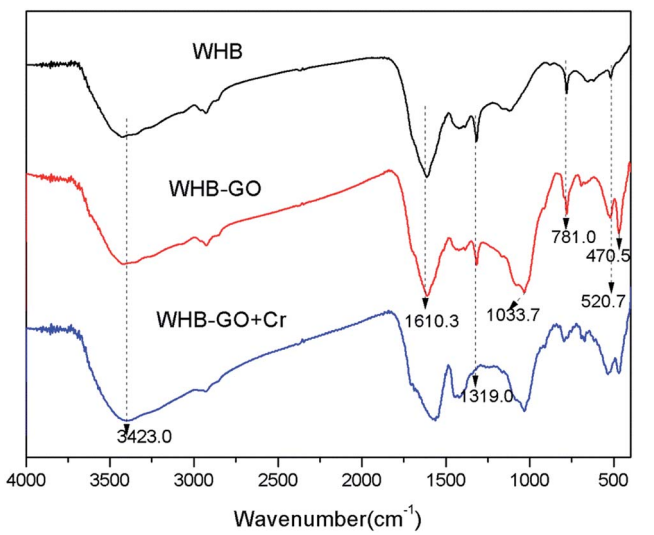


Fig. 2 FT-IR spectra of WHB, WHB-GO and adsorption of Cr(VI) on WHB-GO (WHB-GO + Cr).

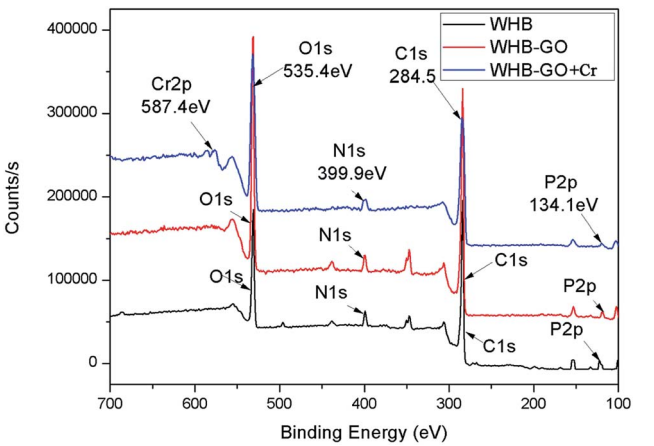


Fig. 3 XPS survey spectra of WHB and WHB-GO before and after adsorption (WHB-GO + Cr).

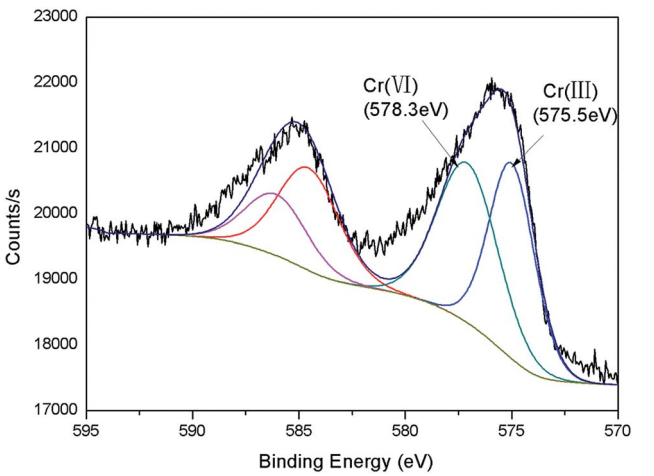


Fig. 4 The Cr 2p XPS spectra of WHB-GO.

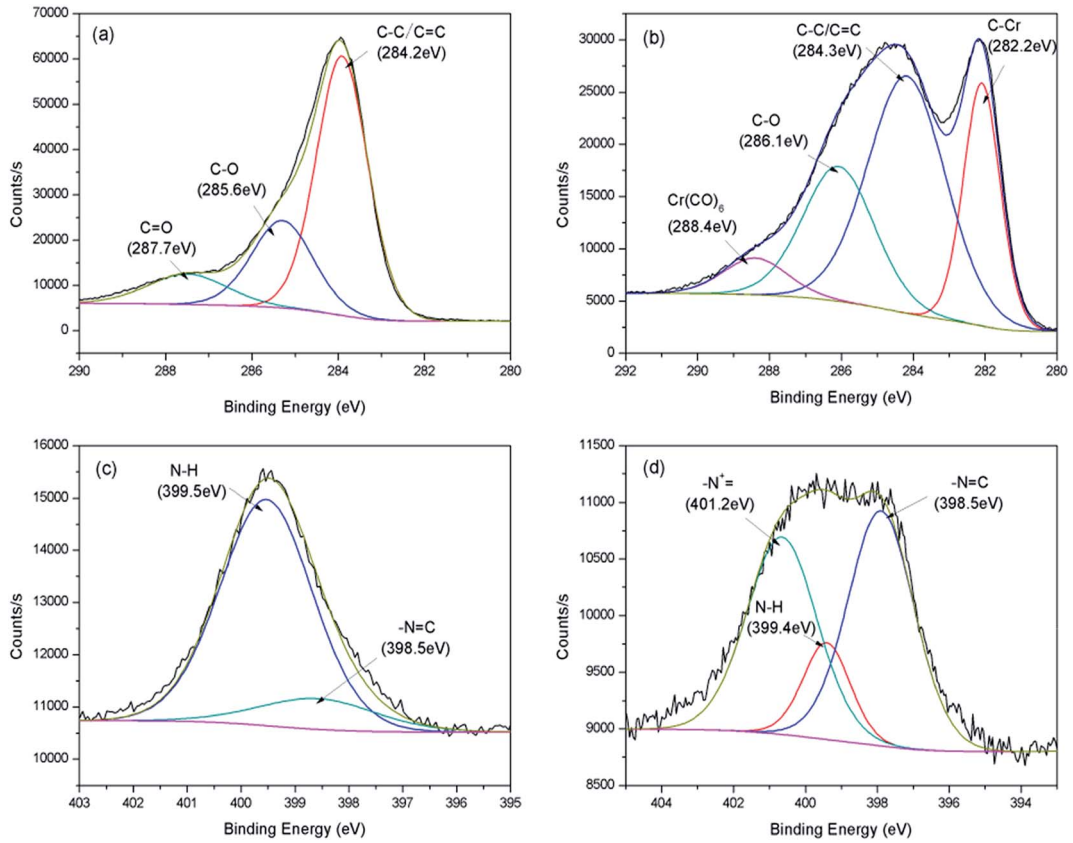


Fig. 5 The C 1s XPS spectra of WHB-GO before (a) and after adsorption (b); the N 1s XPS spectra of WHB-GO before (c) and after adsorption (d).

($K_2Cr_2O_7$).[31] As seen from the Fig. 4, the binding energies at 575.5 and 578.3 eV could be assigned to Cr(III) and Cr(VI), respectively.[32] This suggested that part of adsorbed Cr(VI) anions were reduced to Cr(III) after exposure to WHB-GO. Meanwhile, C 1s bands and N 1s bands of WHB-GO before and after adsorption were also investigated. As seen from Fig. 5(a), three different bands centered at 284.2 eV, 285.6 eV and 287.7 eV were observed corresponding to C–C/C=C, C–O and C=O groups of WHB-GO.[33] The C 1s XPS spectrum of WHB-GO loaded with Cr clearly indicated that four components corresponding to C–Cr (282.2 eV), C–C/C=C (284.3 eV), C–O (286.1 eV) and [$Cr(CO)_6$] (288.4 eV)[34,35] (Fig. 5(b)). Based on the XPS results, the difference between WHB-GO and WHB-GO loaded with Cr might attribute to the introduced carbon functional groups, which enhanced the adsorption ability. As shown in Fig. 5(c), the N 1s XPS spectrum of WHB-GO composite could be curve-fitted into two band components at approximately 398.5 and 399.5 eV, attributable to the –N=C and N–H.[36] After reaction with Cr(VI), a new peak occurred at 401.2 eV, corresponding to nitrogen atoms in doped imine (–$N^+$=)[35] (Fig. 5(d)). It was probably due to the amino groups were involved in the fixation of Cr(VI) and chelation of Cr(III) onto the WHB-GO. According to FT-IR and XPS spectra, the GO was successfully grafted on the biochar surface, which could provide more binding sites for Cr(VI) adsorption.

**3.1.4 BET the BET (Brunauer–Emmett–Teller) surface area, pore volume and average pore size of WHB and WHB-GO were displayed in Table 1.** As shown in Table 1, the BET surface area of WHB-GO (25.89 $m^2\ g^{-1}$) was larger than that of WHB (8.85 $m^2\ g^{-1}$), which could explain that the GO was successfully grafted on WHB and increased the surface area of WHB-GO. However, WHB-GO possessed smaller pore volume and pore size than WHB. The phenomenon might be attributed to the process of preparing WHB-GO, in which water hyacinth biomass was immersed into graphene oxide solution and changed the pore structure of WHB. Besides, the ratio change of some functional groups might constrain $N_2$ in some pore networks and thus the pore volume distribution changed.

Table 1 Selected physical properties of pristine biochar and WHB-GO

| Adsorbent | BET surface, area ($cm^2\ g^{-1}$) | Pore volume ($cm^3\ g^{-1}$) | Pore size (nm) |
|---|---|---|---|
| WHB | 8.85 | 0.025 | 1.716 |
| WHB-GO | 25.89 | 0.019 | 1.613 |

### 3.2 Effect of pH on Cr(VI) adsorption

Solution pH is a significant controlling factor in sorption process. In order to determine the effect of pH on Cr(VI) removal by the WHB-GO, batch adsorption experiments were conducted. Results (Fig. 6) showed that pH ranged from 2.0 to 9.0, the Cr(VI) and total Cr sorption capacities reduced sharply and the

 

maximum adsorption capacity of Cr(VI) was obtained at pH 2.0. Therefore, it was concluded that acidic condition might be more favorable for the Cr(VI) removal by the WHB-GO.

The hexavalent chromium existed in different forms in aqueous solutions at different pH values and Cr(VI) concentrations, such as $H_2CrO_4$ (at pH less than about 1.0), $HCrO_4^-$ (at pH between 1.0 and 6.0) and $CrO_4^{2-}$ (at pH above 6.0).[37]

$$H_2CrO_4 = H^+ + HCrO_4^- \quad (3)$$

$$HCrO_4^- = H^+ + CrO_4^{2-} \quad (4)$$

$$2HCrO_4^- = Cr_2O_7^{2-} + H_2O \quad (5)$$

In other words, the Cr(VI) ions existed mainly in the form of an anion. Fig. 6 illustrated that the adsorption capacity of hexavalent chromium in the solution was lower than total chromium. It was suggested that a part of toxic Cr(VI) might be reduced to the Cr(III) according to the following electron transfer reactions:

$$HCrO_4^- + 7H^+ + 3e^- = Cr^{3+} + 4H_2 \quad (6)$$

$$CrO_4^{2-} + 8H^+ + 3e^- = Cr^{3+} + 4H_2O \quad (7)$$

The zeta potentials of WHB-GO at different pH values were shown in Fig. 7. As shown in Fig. 7, the zeta potential of WHB-GO decreased with the increasing of pH and the zero point of zeta potential ($pH_{pzc}$) was obtained at pH 2.1. At pH < 2.1, the zeta potentials of WHB-GO are positive. At pH > 2.1, the surfaces of WHB-GO are negatively charged. At low pH, the high adsorption capacity could be attributed to the strong electrostatic attraction between the positively charged adsorbent surfaces and the negatively charged chromate ions.[38] With increasing of pH value, the buildup of negative charge on the WHB-GO surfaces resulted in electrostatic repulsion between Cr(VI) ions and the sorbents, which consequently reduced the Cr(VI) sorption.[39] Besides, in high pH solution, the excessive $OH^-$ could compete with Cr(VI) ions for the available adsorption sites on the surface of WHB-GO. Therefore, the initial solution pH 2.0 was used as the optimum pH for the further experiments.

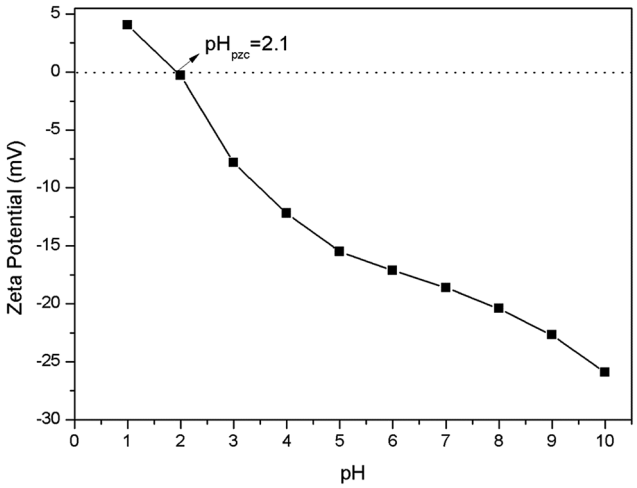


Fig. 7 Zeta potentials of WHB-GO at different solution pH (Cr(VI) solution volume: 50 mL; adsorbent dose: 0.1 g; contact time: 24 h; initial Cr(VI) concentration: 100 mg $L^{-1}$).

### 3.3 Effect of ionic strength on Cr(VI) adsorption

Ionic strength is a very important variable affecting the adsorption of heavy metal ions at aqueous solutions.[40] To investigate the effect of ionic strength on Cr(VI) adsorption, batch experiments at different concentrations of NaCl was conducted. As seen from Fig. 8, the adsorption capacity of Cr(VI) on WHB-GO decreased with the increasing of NaCl concentration from 0.001 to 1 mol $L^{-1}$, which might attribute to the

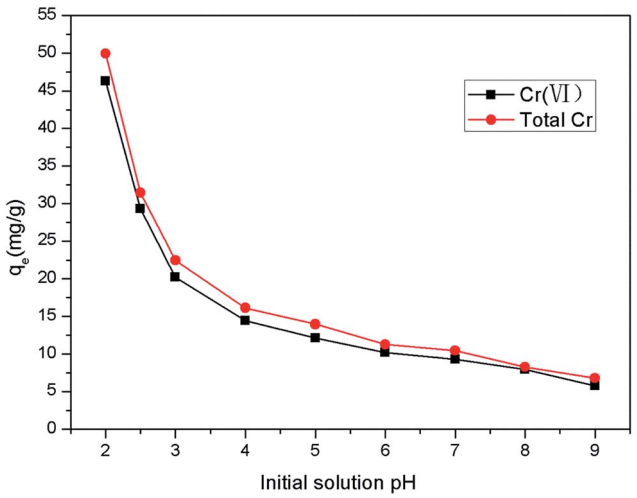


Fig. 6 Effect of initial solution pH values on Cr(VI) and total Cr removal by WHB-GO (Cr(VI) solution volume: 50 mL; adsorbent dose: 0.1 g; contact time: 24 h; initial Cr(VI) concentration: 100 mg $L^{-1}$).

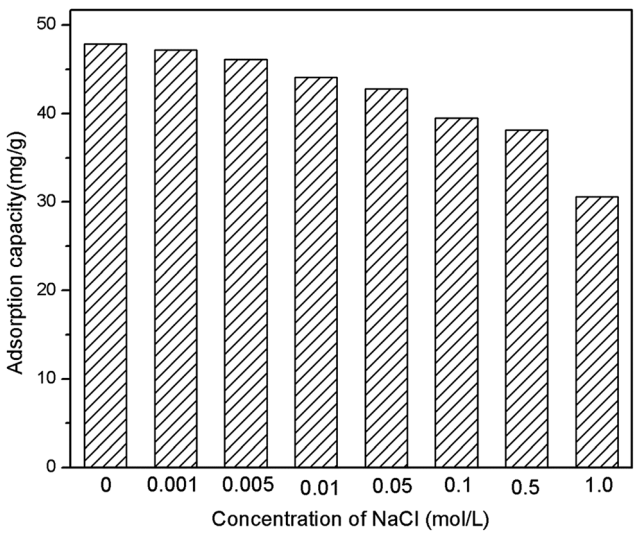


Fig. 8 Effect of different concentrations of NaCl on Cr(VI) removal by WHB-GO (volume: 50 mL; adsorbent dose: 0.1 g; initial Cr(VI) concentration: 100 mg $L^{-1}$; pH: 2.0; contact time: 24 h).

following three possible reasons: (1) $Cl^-$ and $Na^+$ were monovalent ions, they could only slightly compete for the adsorption site of WHB-GO at low concentrations; (2) with the increase concentration of NaCl, the screening effect increased between the negatively charged Cr(VI) in solution and the positively charged adsorbent surface;[41] (3) high concentration of NaCl improved the ionic strength of the solution which led to decrease in the number of collisions between Cr(VI) ions and WHB-GO.[42]

### 3.4 Adsorption kinetics

In order to study the effect of the contact time on adsorption of Cr(VI) by WHB-GO, the adsorption kinetics experiments were carried out. As shown in Fig. 9(a), the removal capacity of Cr(VI) by WHB-GO increased rapidly in the first 6 h, which might due to the abundant availability of active binding sites on the adsorbent surface. And then, the adsorption rate of Cr(VI) became slower and continued a long period of time until sorption equilibrium was attained at 24 h. The slow adsorption process might be explained that the majority of active surface sites were occupied by Cr(VI) ions and there were insufficient binding sites for Cr(VI) to use.

In this research, two mathematical models (pseudo-first-order and pseudo-second-order models) were used to investigate the mechanism of the adsorption process. The equations are generally expressed as follows:[1]

$$\ln(q_e - q_t) = \ln q_e - k_1 t \quad (8)$$

$$\frac{t}{q_t} = \frac{1}{k_2 q_t^2} + \frac{t}{q_e} \quad (9)$$

where $q_e$ and $q_t$ (mg $g^{-1}$) are the adsorption amounts at equilibrium and at any time $t$, respectively, $k_1$ ($min^{-1}$) is the pseudo-first-order reacted rate constant, $k_2$ (g $mg^{-1}$ $min^{-1}$) is the pseudo-second-order reacted rate constant.

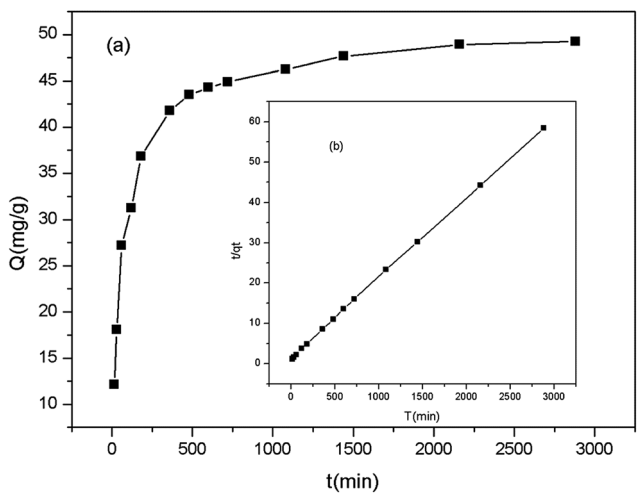


Fig. 9 Kinetics of Cr(VI) adsorption onto the WHB-GO at 30 °C (initial Cr(VI) concentration 100 mg $L^{-1}$; pH: 2.0). (a) Cr(VI) sorption kinetics data; (b) pseudo-second-order model for Cr(VI) adsorption.

The kinetic parameters for Cr(VI) adsorption were calculated by the two models. As can be seen from the Table 2, the correlation coefficients ($R^2$) of the pseudo-first-order and pseudo-second-order equations were 0.92 and 0.99, respectively. What's more, the calculated $q_e$ values (48.84 mg $g^{-1}$) of the pseudo-second-order model were more agreeable to the experimental data than the values of pseudo-first-order model. These results indicated that the pseudo-second-order kinetic model could better fit the adsorption process. Therefore, the mechanism of Cr(VI) sorption by WHB-GO could be the chemical interaction, such as complexation and redox reaction.

### 3.5 Adsorption isotherms

It is important to study the equilibrium adsorption isotherms, since it can provide detailed information to further discuss the adsorption mechanism. In this paper, Langmuir and Freundlich adsorption models were used to simulate the adsorption isotherms data. The Langmuir model assumes monolayer adsorption onto a homogeneous surface with no interactions between the adsorbed molecules. However, the Freundlich models are empirical equations, which are often used to describe the adsorption on a heterogeneous surface without saturation of adsorbent binding sites. The two adsorption models were expressed by the following equations:

$$\frac{C_e}{q_e} = \frac{1}{q_{max} K_L} + \frac{C_e}{q_{max}} \quad (10)$$

$$\ln q_e = \ln K_F + 1/n \ln C_e \quad (11)$$

where $C_e$ and $q_e$ (mg $g^{-1}$) represent the equilibrium concentration and the adsorption capacity at equilibrium, respectively, $q_{max}$ (mg $g^{-1}$) is the maximum adsorption capacity, $K_L$ (L $mg^{-1}$) is the Langmuir constant related to the affinity of the binding sites, $K_F$ (mg $g^{-1}$) is the Freundlich adsorption coefficient and $n$ is an index of isotherm nonlinearity which is related to the adsorption capacity and intensity.

Fig. 10 showed the plots of Langmuir and Freundlich adsorption isotherms of the Cr(VI) on WHB-GO at three different temperatures and the adsorption coefficients were listed in Table 3. As can be seen from the Fig. 10, the adsorption capacity increased with the increase of temperature. The maximum adsorption amount was approximate 150.02 mg $g^{-1}$, which was obtained at the temperature of 50 °C. Table 3 showed that the correlation coefficient ($R^2$) values of Freundlich model (0.98, 0.98 and 0.98) at three temperatures were much better than

Table 2 Pseudo-first-order model and pseudo-second-order model parameters for Cr(VI) adsorption on WHB-GO

| Pseudo-first-order | | Model | Pseudo-second-order | | Model |
|---|---|---|---|---|---|
| $K_1$ ($min^{-1}$) | $q_e$ (mg $g^{-1}$) | $R^2$ | $K_2$ (g $mg^{-1}$ $min^{-1}$) | $q_e$ (mg $g^{-1}$) | $R^2$ |
| 0.013 | 45.41 | 0.92 | $3.8 \times 10^{-4}$ | 48.84 | 0.99 |

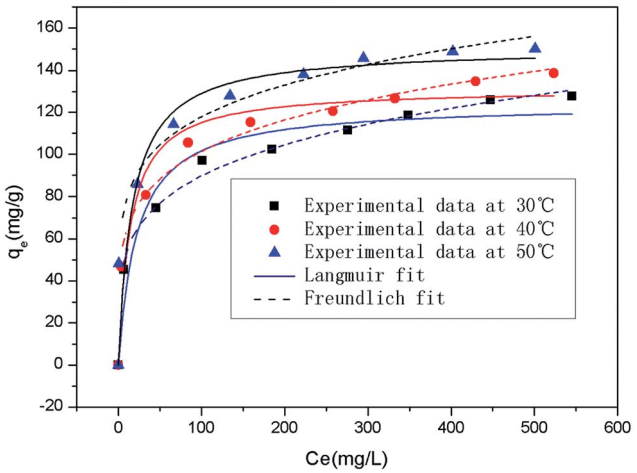


Fig. 10 Langmuir and Freundlich isotherms of Cr(VI) adsorption on WHB-GO (Cr(VI) solution volume: 50 mL; adsorbent dose: 0.1 g; contact time: 24 h; pH: 2.0).

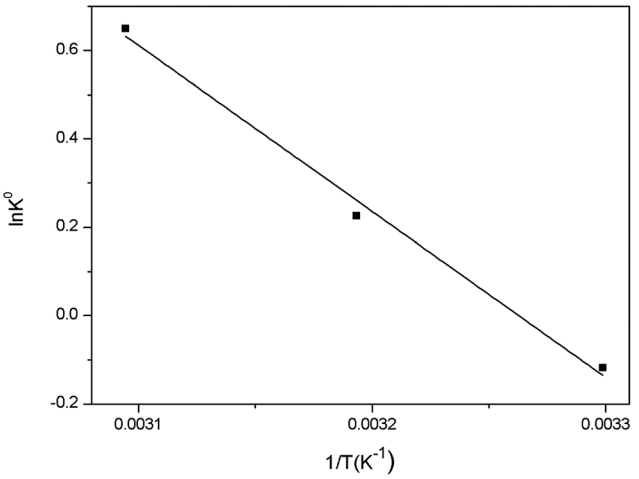


Fig. 11 Plot of ln $k^0$ *versus* 1/$T$ for estimation of thermodynamic parameters for the adsorption of Cr(VI) on WHB-GO (volume: 50 mL; initial Cr(VI) concentration: 100, 200, 300, 400, 500, 600, 700 and 800 mg $L^{-1}$; pH: 2.0; contact time: 24 h).

Table 3 Langmuir and Freundlich isotherm parameters for adsorption of Cr(VI) on WHB-GO

| | Langmuir | Model | | Freundlich | Model | |
|---|---|---|---|---|---|---|
| Adsorbents, $T$ (°C) | $q_m$ (mg $g^{-1}$) | $K_L$ (L $mg^{-1}$) | $R^2$ | $K_F$ (L $mg^{-1}$) | $n$ | $R^2$ |
| 30 | 124.17 | 0.045 | 0.95 | 32.38 | 4.52 | 0.98 |
| 40 | 131.49 | 0.070 | 0.94 | 40.67 | 5.05 | 0.98 |
| 50 | 150.51 | 0.060 | 0.90 | 52.89 | 5.75 | 0.98 |

Table 4 Thermodynamic parameters for Cr(VI) adsorption on WHB-GO

| Temperature (°C) | ln $K^\circ$ | $\Delta G^\circ$ (kJ $mol^{-1}$) | $\Delta H^\circ$ (kJ $mol^{-1}$) | $\Delta S^\circ$ (J $K^{-1}$ $mol^{-1}$) | $R^2$ |
|---|---|---|---|---|---|
| 30 | −0.119 | −2.239 | 31.265 | 102.009 | 0.988 |
| 40 | 0.226 | −3.264 | | | |
| 50 | 0.650 | −5.148 | | | |

those of Langmuir model (0.95, 0.94 and 0.90). Therefore, compared to the Langmuir model, the experimental data were much more suitable for the Freundlich model within the studied temperature range, which suggested that the adsorption of Cr(VI) onto the adsorbent was mainly controlled by the Freundlich surface adsorption mechanisms. The Freundlich model constant $n$ values were range from 4.52 to 5.75, which indicated that the adsorption between metal ions and adsorbent was favorable. The larger value of $n$ could be explained by stronger interaction between adsorbent and heavy metal.[43]

### 3.6 Adsorption thermodynamic studies

To further study the effect of temperature on the adsorption of Cr(VI) ions onto WHB-GO, thermodynamic parameters including Gibbs free energy change ($\Delta G^\circ$), enthalpy change ($\Delta H^\circ$), and entropy change ($\Delta S^\circ$) were calculated by following equations:

$$\Delta G^\circ = -RT \ln K^\circ \quad (12)$$

$$\ln K^\circ = \frac{\Delta S^\circ}{R} - \frac{\Delta H^\circ}{RT} \quad (13)$$

where $R$ (8.314 J $mol^{-1}$ $K^{-1}$) is the universal gas constant, $T$ (K) is the absolute temperature in Kelvin, $K^\circ$ can be calculated by plotting ln $K_d$ ($K_d = q_e/C_e$) *versus* $C_e$ and extrapolating $C_e$ to zero, the values of $\Delta S^\circ$ and $\Delta H^\circ$ can be obtained from the intercept and slope of the ln $K^\circ$ against 1/$T$ (Fig. 11) respectively.

The results on the effect of temperature indicated that the maximum adsorption of Cr(VI) was obtained at 50 °C, and the maximum adsorption capacity ranged from 127.06 mg $g^{-1}$ to 150.02 mg $g^{-1}$ as the temperature increased from 30 °C to 50 °C. The calculated results of thermodynamic parameters for the adsorption of Cr(VI) on WHB-GO were shown in Table 4. As can be seen, the negative values of $\Delta G^\circ$ decrease from −2.239 to −5.148 kJ $mol^{-1}$ with the increase of temperature in the range of 30–50 °C. This phenomenon suggested that the Cr(VI) adsorption process was spontaneous and became more favorable at higher temperatures. The standard changes enthalpy ($\Delta H^\circ$) of the adsorption process was 31.265 kJ $mol^{-1}$, which verified that the adsorption of Cr(VI) ions using the WHB-GO was endothermic in nature. The positive value of $\Delta S^\circ$ suggested that an increased randomness occurred at the solid solution interface during the adsorption process.[44] In short, the sorption process of Cr(VI) onto WHB-GO was endothermic and spontaneous.

### 3.7 Comparison experiments

In order to highlight the superiority of WHB-GO, the comparison experiments of removal efficiency by WHB and water hyacinth biomass were also conducted. As seen from the Fig. 12,

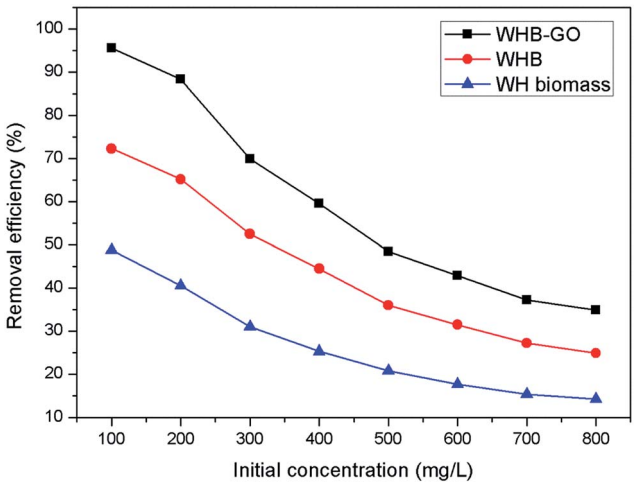


Fig. 12 The comparison of Cr(VI) removal efficiency among the WHB-GO, WHB and WH biomass (Cr(VI) solution volume: 50 mL; adsorbent dose: 0.1 g; contact time: 24 h; pH: 2.0).

the Cr(VI) removal efficiency of the WHB-GO ranged from 95.6% to 34.9%, while the WHB and water hyacinth biomass changed from 72.3% to 24.9% and 48.8% to 14.2%, respectively. Obviously, the removal efficiency of Cr(VI) by the WHB-GO was much higher than WHB and water hyacinth biomass. The high adsorption capacity and removal efficiency of the WHB-GO could be attributed to the introduction of GO molecules, which increased surface areas and multiple functional groups of the adsorbent. A comparison has also been made between the resultant WHB-GO and previously reported adsorbents for maximum Cr(VI) adsorption (Table 5). The results of the analyses demonstrated that this novel functional adsorbent gained advantage over many other adsorbents. It indicated that WHB-GO was a fairly promising candidate for the treatment of chromium-containing wastewater.

### 3.8 Mechanisms of Cr(VI) removal by WHB-GO

As discussed in the effect of pH on Cr(VI) adsorption, the electrostatic attraction is regarded as a adsorption force. However, various types of interactions may also involve in the adsorption process. To verify the adsorption mechanism, the FT-IR spectrums (Fig. 2) and XPS (Fig. 5) of Cr loaded WHB-GO were investigated. The FT-IR spectra corresponding to the WHB-GO loaded with Cr(VI) exhibited an apparent shift in the bending mode at 1610.3 $cm^{-1}$ (C=C) and 781.0 $cm^{-1}$ (aromatic compounds) and the peak of 1319.0 $cm^{-1}$ (C–OH) disappeared. The results indicated that the mechanism of Cr(VI) adsorption onto WHB-GO might rely on the functional groups (C=C, aromatic compounds and C=O) on the material surface. Based on XPS, both Cr(VI) and Cr(III) peaks (Fig. 4) were observed, which implied that the adsorption process involved the reduction of Cr(VI) into Cr(III) with its subsequent partial sorption.

According to the above results, we hypothesized that the adsorption mechanism of Cr(VI) ions by WHB-GO *via* electrostatic attraction of Cr(VI) coupled with Cr(VI) reduction to Cr(III) and Cr(III) complexation.[45] The various mechanisms proposed for the interaction of adsorbent with Cr(VI) were summarized in Fig. 13. Especially, under strongly acidic environment, the removal rate of Cr(VI) in the aqueous phase was faster since the negatively charged Cr(VI) species were migrated to the positively surface of WHB-GO (protonated hydroxyl groups and carbonyl groups) with the help of electrostatic driving forces. While, both direct and/or indirect reduction mechanism(s) involved during the adsorption process. In direct reduction process, Cr(VI) was directly reduced to Cr(III) in the aqueous phase by contact with electron-donor groups of WHB-GO and the reduced-Cr(III) remained in the aqueous solution or formed complexes with Cr-binding groups of it. Indirect reduction mechanism consisted of three steps: (1) the binding of anionic Cr(VI) to positively charged groups present on the surface of WHB-GO; (2) the reduction of Cr(VI) into Cr(III) by adjacent electron-donor groups[31] and (3) the partial release of the reduced-Cr(III) into

Table 5 Adsorption capacities of different adsorbents for Cr(VI)

| Adsorbents | $q_{max}$ (mg $g^{-1}$) | Optimum pH | References |
|---|---|---|---|
| Saw dust activated carbon | 65.8 | 2.0 | 46 |
| Rice husk carbon | 48.31 | 2.0 | 47 |
| CCGO | 67.66 | 2.0 | 48 |
| PEI modified activated carbon | 20.05 | 2.0 | 49 |
| P4VP modified activated carbon | 53.7 | 2.0 | 50 |
| Zinc-biochar nanocomposites | 102.66 | 2.0 | 51 |
| WHB-GO | 150.51 | 2.0 | This study |

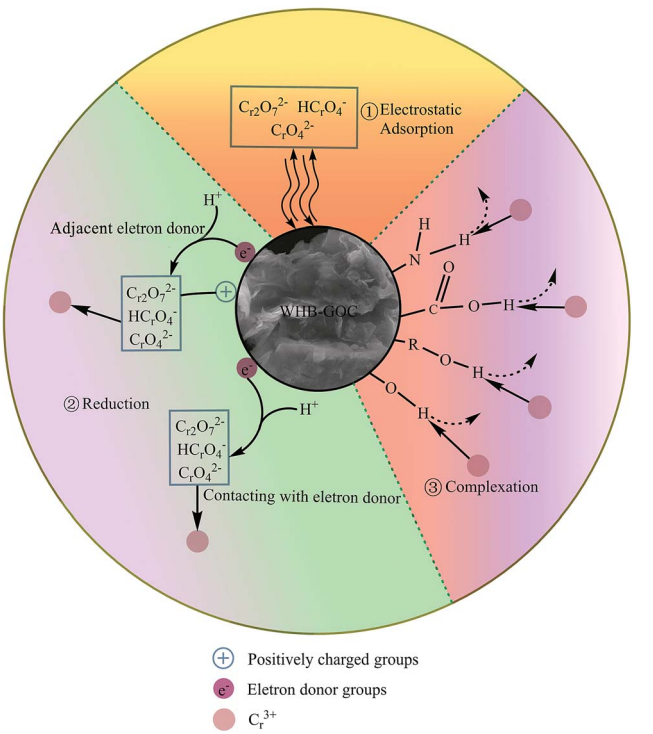


Fig. 13 The schematic illustration of Cr(VI) sorption mechanisms on WHB-GO.

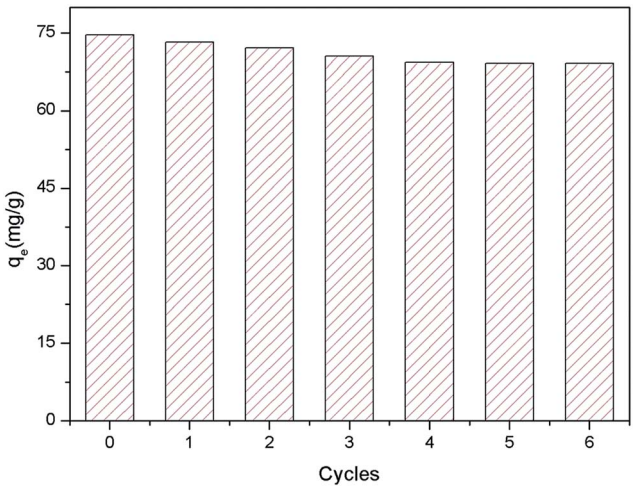


Fig. 14 Sixth consecutive adsorption–desorption cycles of WHB-GO for Cr(VI) removal (volume: 50 mL; adsorbent dose: 0.1 g; initial Cr(VI) concentration: 200 mg $L^{-1}$; pH: 2.0; contact time: 24 h).

the aqueous phase due to electronic repulsion between the positively-charged groups and the Cr(III), or complexation of the reduced-Cr(III) with rest functional groups on the WHB-GO. On the basis of the above analyses, amine, hydroxyl and carbonyl groups could be the main functional groups for Cr(VI) sorption.

### 3.9 Regeneration of WHB-GO

In order to assess the practical utility of the WHB-GO adsorbent, adsorption–desorption experiments were conducted by using 0.5 mol $L^{-1}$ sodium hydroxide and the results were shown in Fig. 14. The results demonstrated that the adsorption activity of WHB-GO only slightly decreased with increasing the number of reuse cycles. The adsorption capacity could still reach 69.10 mg $g^{-1}$ on the sixth reuse cycle, which only reduced by 7.43% compared to that of the first cycle. The excellent regeneration performance indicated that the WHB-GO could be a cost-effective, efficient and potential adsorbent for Cr(VI) removal. In short, the WHB-GO not only had a high adsorption capability, but also possessed a stable performance during the cycles.

## 4. Conclusions

In this work, a new low cost adsorbent was successfully synthesized and applied to remove Cr(VI) from aqueous solution. Results showed that the modification significantly improved the adsorption performance for Cr(VI) removal by combining its adsorption and reduction dual functions. The adsorption capacity was significantly affected by the solution pH and the maximum Cr(VI) adsorption capacity (150.02 mg $g^{-1}$) was obtained at pH 2.0. Background ionic strength exerted obvious influence on the Cr(VI) uptake at the high concentrations of NaCl solution. The experimental data were better fitted by the pseudo-second-order and Freundlich models. Thermodynamic evaluation revealed that the adsorption process was spontaneous and endothermic. Besides, the adsorbent had a good stability during the adsorption–desorption cycles without significant reduction of the adsorption capacity. The results indicated that the new engineered composite can be an innovative and alternative adsorbent, which can effectively and economically remove Cr(VI) ions from aqueous solution.

## Acknowledgements

The authors gratefully acknowledge financial support from the National Natural Science Foundation of China (Grant no. 41271332 and 51478470) and the Hunan Provincial Innovation Foundation for Postgraduate (Grant No. CX2015B090).

## References

1 C. Gan, Y. Liu, X. Tan, S. Wang, G. Zeng, B. Zheng, T. Li, Z. Jiang and W. Liu, *RSC Adv.*, 2015, **5**, 35107–35115.
2 J. J. Pan, J. Jiang and R. K. Xu, *Chemosphere*, 2014, **101**, 71–76.
3 L. Tang, G.-D. Yang, G.-M. Zeng, Y. Cai, S.-S. Li, Y.-Y. Zhou, Y. Pang, Y.-Y. Liu, Y. Zhang and B. Luna, *Chem. Eng. J.*, 2014, **239**, 114–122.
4 N. Adhoum, L. Monser, N. Bellakhal and J. E. Belgaied, *J. Hazard. Mater.*, 2004, **112**, 207–213.
5 A. Hafez and S. El-Mariharawy, *Desalination*, 2004, **165**, 141–151.
6 S. Rengaraj, C. K. Joo, Y. Kim and J. Yi, *J. Hazard. Mater.*, 2003, **102**, 257–275.
7 Y. Pang, G. M. Zeng, L. Tang, Y. Zhang, Y. Y. Liu, X. X. Lei, M. S. Wu, Z. Li and C. Liu, *Bioresour. Technol.*, 2011, **102**, 10733–10736.
8 S. Luo, X. Xu, G. Zhou, C. Liu, Y. Tang and Y. Liu, *J. Hazard. Mater.*, 2014, **274**, 145–155.
9 Y. Wu, H. Luo, H. Wang, C. Wang, J. Zhang and Z. Zhang, *J. Colloid Interface Sci.*, 2013, **394**, 183–191.
10 S. A. Baig, J. Zhu, N. Muhammad, T. Sheng and X. Xu, *Biomass Bioenergy*, 2014, **71**, 299–310.
11 H. Deveci and Y. Kar, *J. Ind. Eng. Chem.*, 2013, **19**, 190–196.
12 D. Mohan, A. Sarswat, Y. S. Ok and C. U. Pittman Jr, *Bioresour. Technol.*, 2014, **160**, 191–202.
13 Z. Hu, X. Ma and L. Li, *Energy Convers. Manage.*, 2015, **94**, 337–344.
14 M.-m. Zhang, Y.-g. Liu, T.-t. Li, W.-h. Xu, B.-h. Zheng, X.-f. Tan, H. Wang, Y.-m. Guo, F.-y. Guo and S.-f. Wang, *RSC Adv.*, 2015, **5**, 46955–46964.
15 Z. Li, T. Katsumi, T. Inui and S. Imaizumi, *Adsorpt. Sci. Technol.*, 2010, **28**, 419–435.
16 P. Liu, W. J. Liu, H. Jiang, J. J. Chen, W. W. Li and H. Q. Yu, *Bioresour. Technol.*, 2012, **121**, 235–240.
17 Y. Feng, H. Zhou, G. Liu, J. Qiao, J. Wang, H. Lu, L. Yang and Y. Wu, *Bioresour. Technol.*, 2012, **125**, 138–144.
18 H. Wang, X. Yuan, Y. Wu, H. Huang, X. Peng, G. Zeng, H. Zhong, J. Liang and M. Ren, *Adv. Colloid Interface Sci.*, 2013, **195–196**, 19–40.
19 J. Xu, L. Wang and Y. Zhu, *Langmuir*, 2012, **28**, 8418–8425.
20 O. Moradi, V. K. Gupta, S. Agarwal, I. Tyagi, M. Asif, A. S. H. Makhlouf, H. Sadegh and R. Shahryari-ghoshekandi, *J. Ind. Eng. Chem.*, 2015, **28**, 294–301.

21 J. Z. Sun, Z. H. Liao, R. W. Si, G. P. Kingori, F. X. Chang, L. Gao, Y. Shen, X. Xiao, X. Y. Wu and Y. C. Yong, *Water Sci. Technol.*, 2014, **70**, 1663–1669.

22 R. Sitko, E. Turek, B. Zawisza, E. Malicka, E. Talik, J. Heimann, A. Gagor, B. Feist and R. Wrzalik, *Dalton Trans.*, 2013, **42**, 5682–5689.

23 J. Wang, Z. Chen and B. Chen, *Environ. Sci. Technol.*, 2014, **48**, 4817–4825.

24 H. Wang, Y.-g. Liu, G.-m. Zeng, X.-j. Hu, X. Hu, T.-t. Li, H.-y. Li, Y.-q. Wang and L.-h. Jiang, *Carbohydr. Polym.*, 2014, **113**, 166–173.

25 P. Avouris and C. Dimitrakopoulos, *Mater. Today*, 2012, **15**, 86–97.

26 H. Yan, X. Tao, Z. Yang, K. Li, H. Yang, A. Li and R. Cheng, *J. Hazard. Mater.*, 2014, **268**, 191–198.

27 J. Liu, G. Liu and W. Liu, *Chem. Eng. J.*, 2014, **257**, 299–308.

28 Z. Wu, H. Zhong, X. Yuan, H. Wang, L. Wang, X. Chen, G. Zeng and Y. Wu, *Water Res.*, 2014, **67**, 330–344.

29 M. Inyang, B. Gao, A. Zimmerman, Y. Zhou and X. Cao, *Environ. Sci. Pollut. Res. Int.*, 2015, **22**, 1868–1876.

30 J. Ma, P. Cai, W. Qi, D. Kong and H. Wang, *Colloids Surf., A*, 2013, **426**, 6–11.

31 D. Park, S. R. Lim, Y. S. Yun and J. M. Park, *Bioresour. Technol.*, 2008, **99**, 8810–8818.

32 H. Cui, M. Fu, S. Yu and M. K. Wang, *J. Hazard. Mater.*, 2011, **186**, 1625–1631.

33 J. N. Tiwari, K. Mahesh, N. H. Le, K. C. Kemp, R. Timilsina, R. N. Tiwari and K. S. Kim, *Carbon*, 2013, **56**, 173–182.

34 W. Xu, S. Wang, Y. Liu, G. Zeng, B. Zheng, X. Tan, T. Li, H. Wang, F. Guo and M. Zhang, *RSC Adv.*, 2015, **5**, 24009–24015.

35 G. Yang, L. Tang, Y. Cai, G. Zeng, P. Guo, G. Chen, Y. Zhou, J. Tang, J. Chen and W. Xiong, *RSC Adv.*, 2014, **4**, 58362–58371.

36 G. X. Yang and H. Jiang, *Water Res.*, 2014, **48**, 396–405.

37 D. Mohan and C. U. Pittman Jr, *J. Hazard. Mater.*, 2007, **142**, 1–53.

38 M. QuiIntana, G. Curutchet and E. Donati, *Biochem. Eng. J.*, 2001, **9**, 11–15.

39 X. Dong, L. Q. Ma and Y. Li, *J. Hazard. Mater.*, 2011, **190**, 909–915.

40 T. S. Anirudhan and M. Ramachandran, *Ind. Eng. Chem. Res.*, 2008, 47.

41 F.-y. Guo, Y.-g. Liu, H. Wang, G.-m. Zeng, X.-j. Hu, B.-h. Zheng, T.-t. Li, X.-f. Tan, S.-f. Wang and M.-m. Zhang, *RSC Adv.*, 2015, **5**, 45384–45392.

42 Z.-b. Zhang, X.-h. Cao, P. Liang and Y.-h. Liu, *J. Radioanal. Nucl. Chem.*, 2012, **295**, 1201–1208.

43 M. Lu, Y.-g. Liu, X.-j. Hu, Y. Ben, X.-x. Zeng, T.-t. Li and H. Wang, *J. Cent. South Univ.*, 2013, **20**, 2478–2488.

44 G. Zhao, J. Li and X. Wang, *Chem. Eng. J.*, 2011, **173**, 185–190.

45 D. Park, Y. S. Yun, J. H. Jo and J. M. Park, *Water Res.*, 2005, **39**, 533–540.

46 T. Karthikeyan, S. Rajgopal and L. R. Miranda, *J. Hazard. Mater.*, 2005, **124**, 192–199.

47 M. Bansal, D. Singh and V. K. Garg, *J. Hazard. Mater.*, 2009, **171**, 83–92.

48 L. Li, L. Fan, M. Sun, H. Qiu, X. Li, H. Duan and C. Luo, *Colloids Surf., B*, 2013, **107**, 76–83.

49 M. Owlad, M. K. Aroua and W. M. Wan Daud, *Bioresour. Technol.*, 2010, **101**, 5098–5103.

50 J. Fang, Z. Gu, D. Gang, C. Liu, E. S. Ilton and B. Deng, *Environ. Sci. Technol.*, 2007, **41**, 4748–4753.

51 C. Gan, Y. Liu, X. Tan, S. Wang, G. Zeng, B. Zheng, T. Li, Z. Jiang and W. Liu, *RSC Adv.*, 2015, **5**, 35107–35115.